Sheffield
Hallam
University

Enhanced thermal stability of high-bismuth borate glasses by addition of iron

MARY, Nicolas, REBOURS, Marius, CASTEL, Elena, VAISHNAV, Shuchi, DENG, Wei, BELL, Anthony, CLEGG, Francis <http://orcid.org/0000-0002-9566-5739>, ALLSOPP, Benjamin, SCRIMSHIRE, Alex and BINGHAM, Paul <http://orcid.org/0000-0001-6017-0798>

Available from Sheffield Hallam University Research Archive (SHURA) at:

http://shura.shu.ac.uk/22353/

This document is the author deposited version. You are advised to consult the publisher's version if you wish to cite from it.

Published version

Copyright and re-use policy

Sheffield Hallam University Research Archive
http://shura.shu.ac.uk

Enhanced thermal stability of high-bismuth borate glasses by addition of iron

N. Mary[1], M. Rebours[1], E. Castel[1], S. Vaishnav[1], W. Deng[1], A. M. T. Bell[1], F. Clegg[1], B. L. Allsopp[1], A. Scrimshire[1] and P. A. Bingham[1],*

[1] Materials and Engineering Research Institute, Faculty of Arts, Computing, Engineering and Sciences, Sheffield Hallam University, City Campus, Howard Street, Sheffield S1 1WB, UK

Abstract

Glasses with nominal molar composition $20B_2O_3 - (80\text{-}x)Bi_2O_3 - xFe_2O_3$ (where x = 0–40) were successfully prepared by melt-quenching. These glasses were characterised by multiple techniques including density, X-ray diffraction (XRD), X-Ray fluorescence (XRF), Raman, FT-IR and Mössbauer spectroscopies, dilatometry and differential thermal analysis (DTA). Partial replacement of Bi_2O_3 by Fe_2O_3 leads to decreasing density and molar volume and a substantial increase in thermal stability, as measured by several parameters, with maximum improvements achieved when x = 10-20. These improvements are accompanied by modest increases in dilatometric softening point. FT-IR and Raman spectra confirm the presence of BO_3 and BiO_6 structural units in all glasses, with glass structure apparently little affected by Fe_2O_3. Mössbauer spectroscopy confirms that iron is present partly as 4-fold coordinated Fe^{3+} in all glasses, with some 5- and / or 6- coordinated Fe^{3+} sites also present.

* Corresponding Author. Email p.a.bingham@shu.ac.uk

1. Introduction

Low-melting glasses have a wide range of applications and are essential to providing hermetic sealing in many applications including electronic, semiconducting, optical and photovoltaic devices, amongst many others [1-4]. Some of the lowest-melting and lowest-sealing temperature glasses, often referred to as solder glasses, were traditionally based on the lead borate system [1-4]. Freiser [2] noted that the viscosity-temperature profile of solder glasses should be such that the "preferred zone" of viscosity enabling viscous flow of the solder glass, should leave the work piece (metal or glass) unaffected. Takamori [3] considered solder glasses

on the basis of their thermal expansion coefficient. However, in recent years legislation has effectively banned the use of lead in sealing glasses [1] and in many other glasses, and manufacturers continue to search for alternative, lead-free sealing glasses capable of delivering low sealing temperatures and acceptable thermal expansion behaviour.

Other low-melting borate glasses include alkali borates [5-8] and in order to access glass transition temperatures, T_g, of < 573K, alkali borate glasses with high alkali contents are required [6]. However, such high-alkali glasses display high thermal expansion coefficients ($15 - 25$ x 10^{-6} K^{-1}) [6], which will render them unsuitable for some sealing applications. Lower alkali borate glasses exhibit T_g's of ca. 623 - 723 K [8]. Binary alkaline earth borate glasses and ternary alkali-alkaline earth borate glasses exhibit even higher values of T_g, as discussed by Wozniak and James [9]. Furthermore, alkali borate glasses exhibit poor chemical durability and are therefore less attractive as potential lead-free sealing glasses. Zinc in borate sealing glasses has also received considerable attention [1-4], however, ZnO was traditionally a third component in B_2O_3-PbO glasses and comparable high-zinc glasses in the binary B_2O_3-ZnO system typically exhibit higher T_g's > 773 K, too high for some sealing applications.

One family of glasses that may be capable of replacing lead with a non-toxic alternative in some applications occurs in the B_2O_3-Bi_2O_3 system. In his recent, very thorough review of bismuth-containing glasses Maeder [1] noted that Bi_2O_3 "appears a quite promising drop-in replacement for PbO" but "the somewhat lower fluxing ability…..leads to higher processing temperatures". Despite this, bismuth-rich low temperature sealing glasses have been successfully developed [10-12]. Bismuth borates have been stated to form transparent glasses over a particularly wide range of Bi_2O_3 contents, from 20 to 85 mol% [13]. Bajaj *et al.* [13] undertook a detailed investigation of the structure and properties of glasses in the system $xBi_2O_3 - (100-x)B_2O_3$ where x = 20 to 66 (mol %), and noted the interest in this system for non-linear optics. Shaaban *et al.* [14] studied glasses with compositions $xBi_2O_3 - (100 - x)B_2O_3$ where x = 35 to 60 mol%. They carefully characterised thermal properties, crystallisation behaviour and structure, demonstrating that thermal stability decreased with increasing Bi_2O_3 content.

A wide range of additional components to the B_2O_3-Bi_2O_3 glass system has been studied previously, as summarised by Maeder [1]. However, a dopant that has received relatively little attention, particularly in the context of high-bismuth sealing glasses, is iron. Dumbaugh [15] showed that the binary system Bi_2O_3-Fe_2O_3, which contains no classical glass formers, is capable

of forming glasses over a considerable range of iron contents, given the inclusion of a third component (in Dumbaugh's case CdO and / or PbO). This offered a tantalising clue to the potential for incorporating iron in high-bismuth glasses. Qiu *et al.* [16] studied glass formation and DC conductivity in the system B_2O_3-Bi_2O_3-Fe_2O_3, and confirmed that high-Bi_2O_3, low-B_2O_3 glasses containing up to 40 mol % Fe_2O_3 can be formed by press-quenching the melt between two copper blocks. Baia *et al.* [17, 18] studied the structure of a wide range of compositions in the systems (mol%) 95[xB_2O_3.(1-x)Bi_2O_3]-5Fe_2O_3 where $0.07 \leq x \leq 90$ and 90[xB_2O_3.(1−x)Bi_2O_3]-10Fe_2O_3 where $0.07 \leq x \leq 0.625$ using Raman and FT-IR spectroscopies. They found that Bi^{3+} cations are incorporated in the glass network as BiO_6 polyhedra, and iron doping can stabilise the glass network at intermediate bismuth contents. El-Desoky and colleagues [19-21] studied doping of iron into B_2O_3-Bi_2O_3-R_2O (R=Li, Na, K) glasses, however, they were primarily investigating electrical properties and their glasses were relatively high in B_2O_3 and low in Bi_2O_3. Akamatsu *et al.* [22] studied the magnetic and structural properties of glasses with nominal molar composition xFe_2O_3 - (80 − x) Bi_2O_3 -·20 B_2O_3 (where x = 18.2 - 40.0). These glasses exhibit unusual magnetic behaviour which they explained in terms of coexisting spin glass phases and magnetic clusters. Another application area of interest in high-bismuth glasses is for radiation shielding / dosimeter applications, and these have also received recent attention [23 - 24]. The presence of boron and bismuth could enable potential applications in the nuclear arena, due to the high absorption cross-section for thermal-neutrons (B) and γ-radiation (Bi). In terms of iron-free bismuth borate glasses, Yawale and Pakade [25] studied the physical and electrical transport properties of Bi_2O_3-B_2O_3 glasses, and further detailed studies of the physical properties of Bi_2O_3-B_2O_3 glasses, across a wide range of compositions, were carried out by Stehle *et al.* [26] and George *et al.* [27]. The high densities of bismuth-rich borate glasses are inherently linked to all of the above applications. As noted by Maeder [1], anomalies in density and T_g can also suggest structural information, hence knowledge of the density and molar volume of bismuth borate glasses is important. One additional property requirement of sealing glasses is that they exhibit sufficient chemical durability for the application in question. As discussed by Maeder [1], some high-lead borate glasses and high-bismuth borate glasses exhibit chemical durabilities that are considered acceptable for many low-temperature sealing applications.

Understanding the effects of iron additions to the structure and properties of high-bismuth borate glasses is therefore of interest, not only from the perspective of developing new lead-free sealing glasses, but also within the wider context of understanding the structure of high-bismuth oxide glasses, and in terms of new potential applications requiring novel electrical, nuclear or other properties. Here we have studied the effects of iron doping on the structure and physical properties of glasses with nominal molar composition $20\ B_2O_3 - (80\text{-}x)\ Bi_2O_3 - xFe_2O_3$ (where x = 0–40).

2. Experimental Procedures

Batches to provide 50g of glass were produced using the reagent-grade chemicals boric acid (H_3BO_3, 99.5%), bismuth oxide (Bi_2O_3, 99%) and iron oxide (Fe_2O_3, 98%). Raw materials were carefully dried overnight prior to weighing (H_3BO_3 at 323 K so as not to decompose; and Bi_2O_3 and Fe_2O_3 at 393 K). Batches were weighed out using a calibrated 2 decimal-place balance, and were then mixed thoroughly. Nominal glass compositions are listed in Table 1. The mixed batches were then placed in recrystallised Al_2O_3 crucibles, with an Al_2O_3 lid placed over the crucible to reduce volatilisation losses during heating and melting. Crucibles were placed in an electric furnace and heated at 5 K / min in air to 1373 K, and held at this temperature for 30 minutes. The lids were then removed from the crucibles and the crucibles removed from the furnace and their contents press-quenched between two steel plates. Resulting samples were then stored in sealed bags. Samples were powdered in an attrition mill for 1 minute to provide samples for XRD, XRF, Mössbauer spectroscopy, DTA and FT-IR spectroscopies. Density measurements, Raman spectroscopy and dilatometry were performed on bulk glass samples.

Densities have been measured by the Archimedes method using deionised water as the suspension medium. Archimedes densities are calculated using (1):

$$\text{Density} = ((W_A / (W_A - W_W)) \text{ x } \delta_W \qquad (1)$$

where W_A = weight in air, W_W = weight in water and δ_W = temperature correction. Averages of three measurements were taken for each sample. Molar volumes have been calculated using measured densities and analyzed compositions.

Elemental analysis was performed using a PANalytical MagiX Pro XRF spectrometer equipped with a Rh anode. Powdered samples were mixed with cellulose binder and pressed into pellets using a 20 tonne force in a Retsch PP40 hydraulic press. A semi-quantitative XRF analysis program, IQ+ for standardless data analysis, was used here. Boron was not detected by XRF and so to enable useful analysis it had to be assumed that no boron losses had occurred during melting, and analysed content was modified to take account of the presence of boron on a pro rata basis. Accuracies of the resultant data in this study, arising from the use of the semi-quantitative analysis program, are estimated to be ±3 of their values as provided by the analysis, based on historical results using this instrument and analysis program on other, related glasses.

X-ray diffraction was performed at room temperature on powdered pellets using an Empyrean PANalytical diffractometer in Bragg–Brentano geometry. Samples were mounted on a reflection/transmission spinner stage rotating at 15 rpm, irradiated with Cu Kα radiation (λ = 1.5406 Å) over a °2θ range of 20–80°, with step size 0.013 °2θ and step time 68.59 s, 10 mm incident mask, 1° antiscatter and divergence slits, and a nickel beta filter. X-rays were detected using a PIXCEL-3D area detector.

Dual DTA and TGA analysis of the sample were carried using a NETZSCH STA 409 PC/PG, with 180mg of powdered sample in air. Measurements were carried out at a heating rate of 10^oC / minute from 50°C to 780°C. No detectable changes in sample mass during analysis were noted, within the uncertainties of the instrument. The temperatures T_g (glass transition temperature), T_x (onset crystallization temperature) and T_c (crystallization peak temperature) were determined from the corrected DTA traces, which are shown in Figure 2. The extracted T_g, T_x and T_c temperatures are given in Table 1 Uncertainties associated with each of the above measured parameters (+/- 3K) were estimated from repeat measurements of the same sample and temperature calibration of the instrument using a standard. Thermal stabilities and glass-forming abilities of the glasses were estimated using three different methods: $\Delta T = (T_x - T_g)$ [28]; $S = (T_c - T_x) (T_x - T_g)/(T_g)$ [29]; and the Hrubý parameter, $K_{gl} = (T_x - T_g) / (T_m - T_x)$ [30]. Figure 3 shows T_g and $\Delta T = (T_x - T_g)$ as functions of nominal Fe_2O_3 content.

Dilatometry was carried out using a Netzsch Expedis Select dilatometer at a heating rate of 5 K / min from 293 K to a temperature above the dilatometric softening point, T_d. Owing to the press-quenching method used to produce the glass samples and their resulting thickness of ~1 mm, it was only possible to obtain T_d values from dilatometry and not coefficient of thermal

expansion, α. The obtained T_d values are shown in Table 1. Uncertainties associated with measured T_d (+/- 3K) were estimated from repeat measurements of the same sample and temperature calibration of the instrument using a standard.

Fourier-Transform Infra-Red (FT-IR) spectroscopy was carried out using a Nicolat Nexus 470 FT-IR spectrometer. Powdered glass samples were mixed with dry KBr and pressed into pellets using a pellet press, for transmission measurements. Spectra were recorded between 600 and 1800 cm^{-1}, and are shown in Figure 4.

Raman spectroscopy was carried out using a Thermo Scientific DXR2 spectrometer with a depolarised 10 mW 532 nm laser, on bulk samples of all glasses, between 200 and 2000 cm^{-1}. Calibrations with the proprietary Thermo alignment tool were carried out before, during and after each sample measurement. Spectra were baseline-corrected and are shown in Figure 5 and key Raman band assignments associated with the spectral features are summarised in Table 3. There is a strong damping effect, such that most spectral features were increasingly suppressed upon increasing Fe_2O_3 content of the glasses. The spectra shown in Figure 5 have thus been progressively amplified in order to illustrate spectral features, which explains the progressively lower signal-to-noise (S/N) ratio with increasing Fe_2O_3 content of the samples.

Transmission ^{57}Fe Mössbauer spectroscopy measurements were carried out using acrylic absorber discs with a sample area of 1.767 cm^2. These were loaded with sample to present 2.16 $\times$ 10^{-3} g cm^{-2} of Fe to achieve a Mössbauer thickness of 1. Sample weights of 0.013 g were homogeneously mixed with graphite to achieve this level of loading. The 14.4 keV γ-rays were supplied by the cascade decay of 25 mCi ^{57}Co in Rh matrix source, oscillated at constant acceleration by a SeeCo W304 drive unit, and detected using a SeeCo 45431 Kr proportional counter operating with 1.745 kV bias voltage applied to the cathode. All measurements were carried out at room temperature over a velocity range of ±4 mm s^{-1}, and were calibrated relative to α-Fe foil. Spectral data were fitted using the Recoil software package [31], using Lorentzian line shapes. The low S/N obtained for each sample was caused by strong absorption of incident gamma-rays by the sample (due to very high bismuth contents). Long collection times of up to 3 weeks were required for each sample, and consequently spectral fitting was limited to a single doublet for each spectrum. Attempts were made to fit two doublets, however, these resulted in no significant improvement in reduced χ² for each fit and were consequently discarded in favour of single-doublet fits.

3. Results

      Table 1 shows the nominal and analysed glass compositions studied, with sample name nomenclature (0Fe, 10Fe, 20Fe, 30Fe, 40Fe) reflecting the nominal molar percentage Fe_2O_3 content. X-ray diffraction confirmed the X-ray amorphous nature of all samples. Standardless XRF analysis confirms that all of our glasses contain ~1 to 2 wt% (~ 4 to 7 mol%) Al_2O_3, as shown in Table 1. These Al_2O_3 contents are attributed to unavoidable chemical interactions of the molten glass with the Al_2O_3 crucibles during melting. Due to the very high Bi_2O_3 contents of these glasses (which strongly re-absorb emitted X-rays), combined with the semi-quantitative nature of the standardless XRF analysis program used, there are considerable uncertainties associated with the XRF analyses, as shown in Table 1. Measured densities and corresponding molar volumes, shown in Table 1 and Figure 1, depict monotonic decreases and increases, respectively, in density and molar volume with increasing Fe_2O_3 content.

Table 1. Nominal (analysed) glass compositions, density, molar volume and thermal parameters.

Sample	Nominal (analysed) composition/mol%				Density, ρ/g cm⁻³ (± 0.01)	Molar Vol., V_m cm⁻³ (± 0.5)	T_g / K (± 3)	T_x / K (± 3)	T_c / K (± 3)	T_m / K (± 3)	ΔT / K (±6) [28]	S [29]	K_{gl} [30]	T_d / K (±3)
	B_2O_3	Fe_2O_3 (± 3)	Bi_2O_3 (± 3)	Al_2O_3 (± 3)										
0Fe	20.0*	0.0 (0.0)	80.0 (73.7)	0.0 (6.3)	7.88	49.1	603	635	655	861	32	1.06	0.142	600
10Fe	20.0*	10.0 (6.8)	70.0 (65.9)	0.0 (7.3)	7.58	47.0	635	701	715	858	66	1.46	0.420	635
20Fe	20.0*	20.0 (14.5)	60.0 (61.0)	0.0 (4.5)	7.25	44.9	662	723	755	923[a]	61	2.95	0.305[a]	665
30Fe	20.0*	30.0 (21.5)	50.0 (52.7)	0.0 (5.7)	6.99	42.2	692	731	752[a]	948[a]	39	1.18	0.180[a]	675
40Fe	20.0*	40.0*	40.0*	0.0*	6.63	39.9	690	745	777[a]	904[a]	55	2.55	0.346[a]	680

* not measured; [a] DTA traces showed multiple phase formation / melting.

8

Figure 1. Measured densities and estimated molar volumes for samples 0Fe to 40Fe. Lines are shown as a guide. Error bars are smaller than data points.
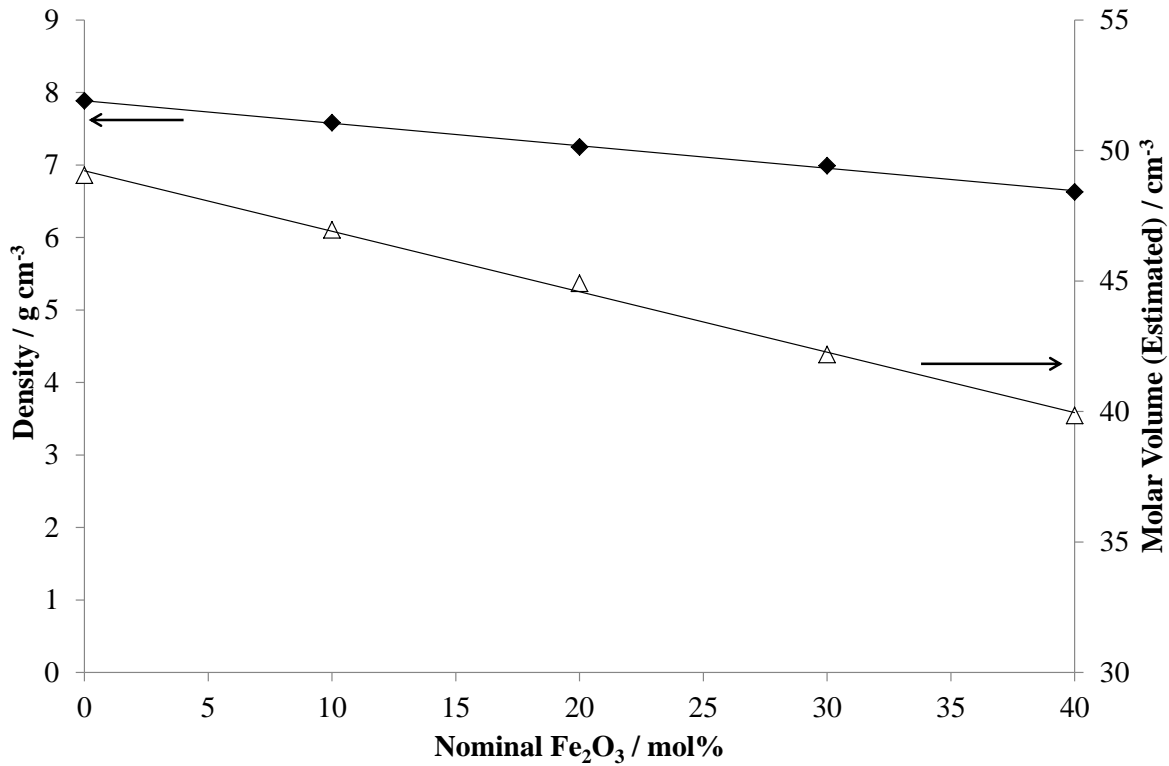
Differential Thermal Analysis (DTA) traces, shown in Figure 2, and the extracted and calculated thermal parameters given in Table 1, depict clear trends in T_g, the glass transition temperature; in T_x, the onset crystallisation temperature, and in T_c, the peak crystallisation temperature, for this series of glasses. T_g, T_x and T_c all increase with increasing nominal Fe_2O_3 content, but ΔT, the temperature difference between T_x and T_g ($\Delta T = T_x - T_g$), varies with glass composition.. This behaviour is tabulated in Table 1 and shown graphically in Figure 3 for T_g and the temperature difference between T_x and T_g ($\Delta T = T_x - T_g$). Figure 2 also shows a clear endothermic event, associated with melting, for the 0, 10 and 20 mol% Fe_2O_3 glasses. This endotherm moves to slightly lower temperatures with iron additions, from ca. 888 K at 0 mol % Fe_2O_3 to ca. 863 K at 20 mol% Fe_2O_3. At higher Fe_2O_3 additions, this endothermic event disappears and with increasing iron content the high-temperature region of the DTA traces becomes increasingly complex. In addition to thermal stability related factors, high temperature viscosity (as measured by dilatomeric softening point, T_d) shows a monotonic increase from

9

600K at 0 mol% Fe_2O_3 to 635K at 10 mol% Fe_2O_3 to 665K at 20 mol% Fe_2O_3. At higher Fe_2O_3 the rate of increase in T_d decreases, with T_d of 675K at 30 mol% Fe_2O_3 and 680K at 40 mol% Fe_2O_3.

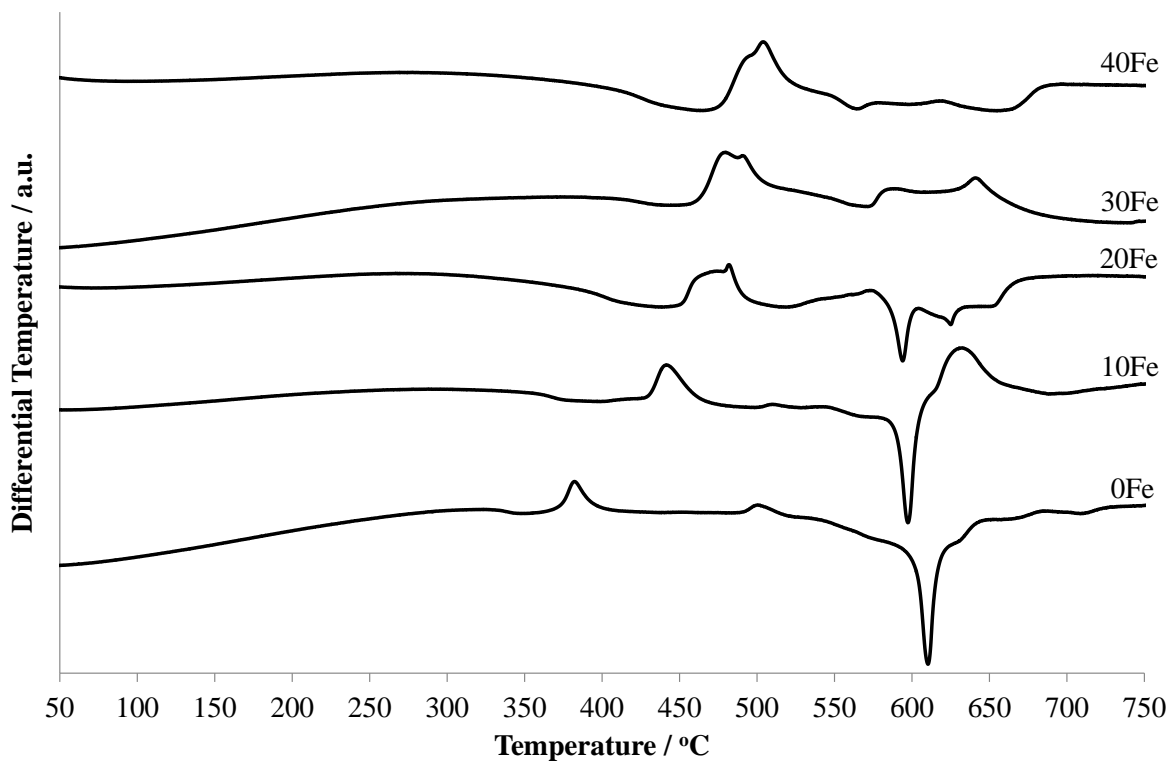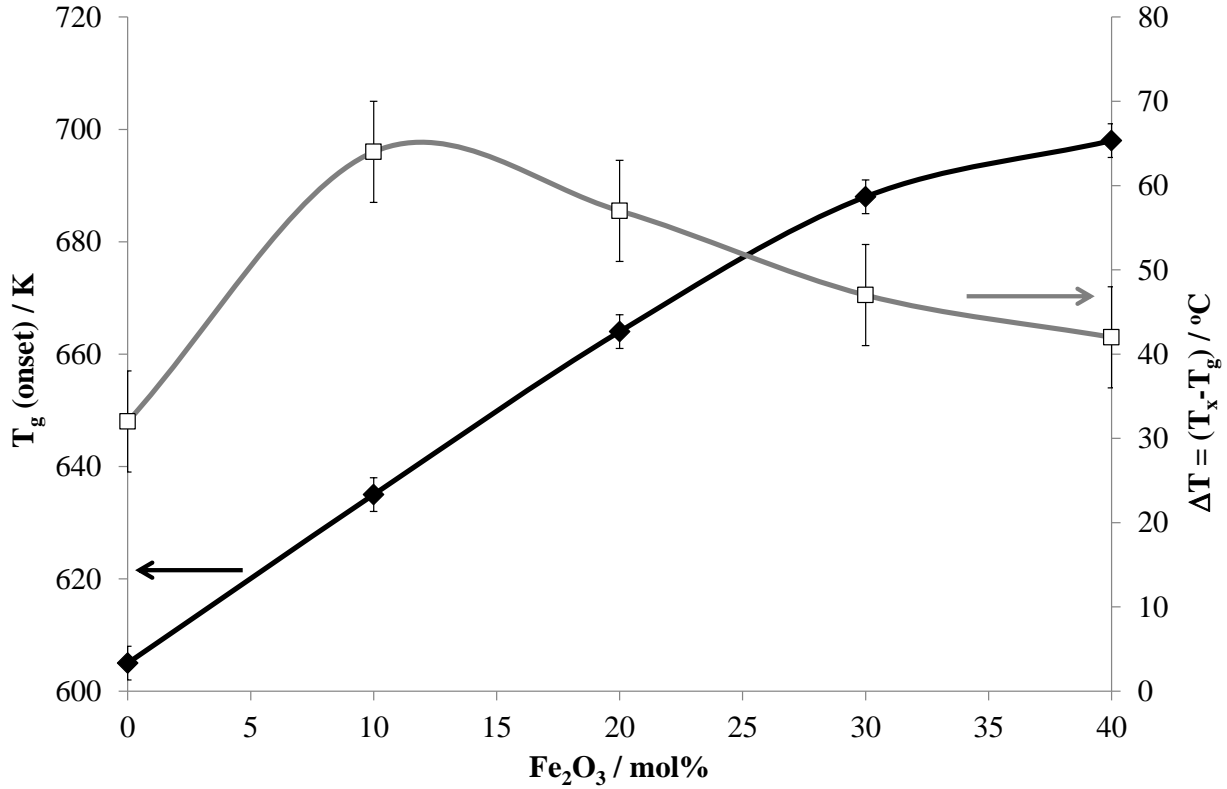*Figure 2.* DTA traces for samples 0Fe to 40Fe

Figure 3. Onset T_g and thermal stability (T_x-T_g) as functions of nominal Fe_2O_3 content

Fourier-Transform Infra-Red (FT-IR) transmission spectra, shown in Figure 4, evidence little change throughout the series of glasses. Absorption bands are as follows: (i) a narrow band centred at 720 cm^{-1}; (ii) a broad, weak band centred at 920 cm^{-1+}; (iii) a strong, broad band centred at 1180 cm^{-1}; and (iv) a weaker shoulder at 1280 cm^{-1}. Raman spectra for all samples (Figure 5) all exhibit the following bands: (i) a broad band centred at 400 cm^{-1}; (ii) a broad band at 600 cm^{-1}; (iii) a weak, narrow band at 710 cm^{-1}; (iv) a sharp band at 840 cm^{-1}; (v) a weak band at 920 cm^{-1}; and (vi) a broad band centred at 1230 cm^{-1} comprising two overlapping bands centred at 1180 cm^{-1} and 1280 cm^{-1}. Table 2 summarises FT-IR and Raman band assignments and provides supporting references.

Mössbauer spectra (Figure 6) and accompanying fitted parameters (Table 3) show closely similar Centre Shift (CS), Quadrupole Splitting (QS) and Linewidth (LW) values for all three samples studied, containing nominally 20, 30 and 40 mol% Fe_2O_3, indicating little or no change in the oxidation state or local environment of Fe cations with changing glass composition.
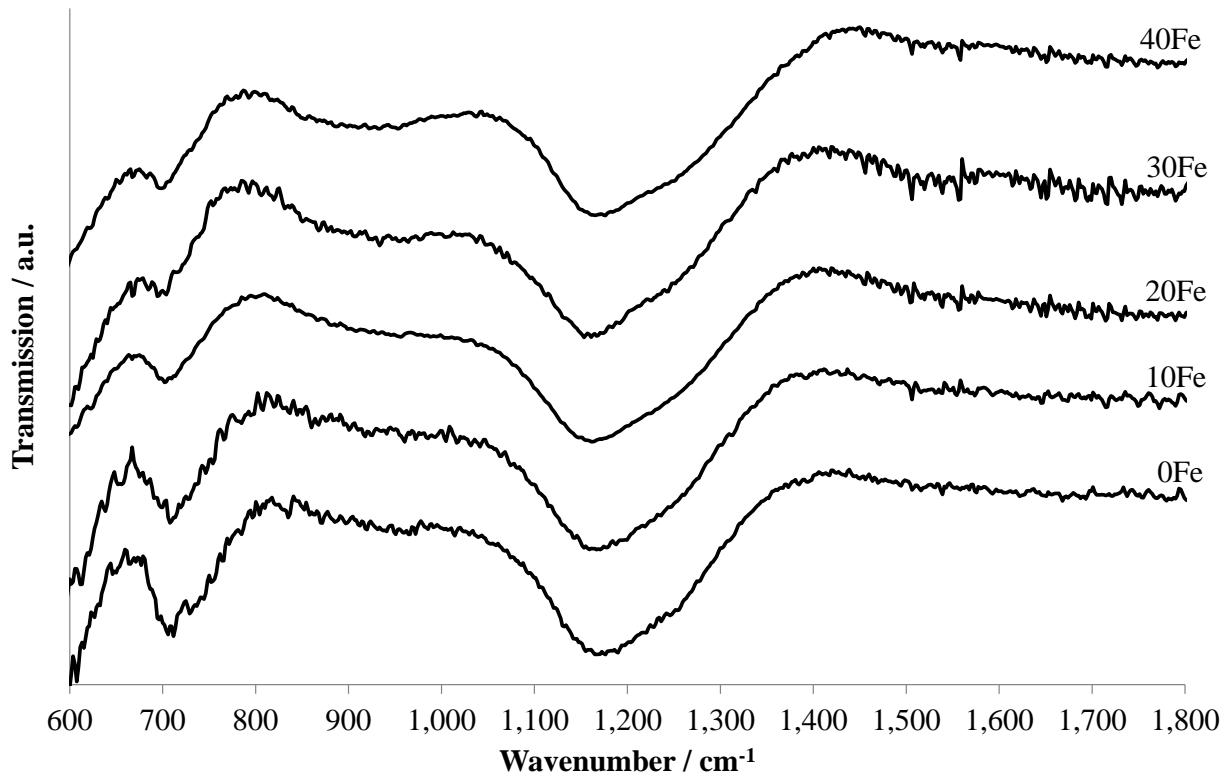
Figure 4. FT-IR spectra for samples 0Fe to 40Fe

Figure 5. Raman spectra for samples 0Fe to 40Fe (amplified with increasing Fe content)
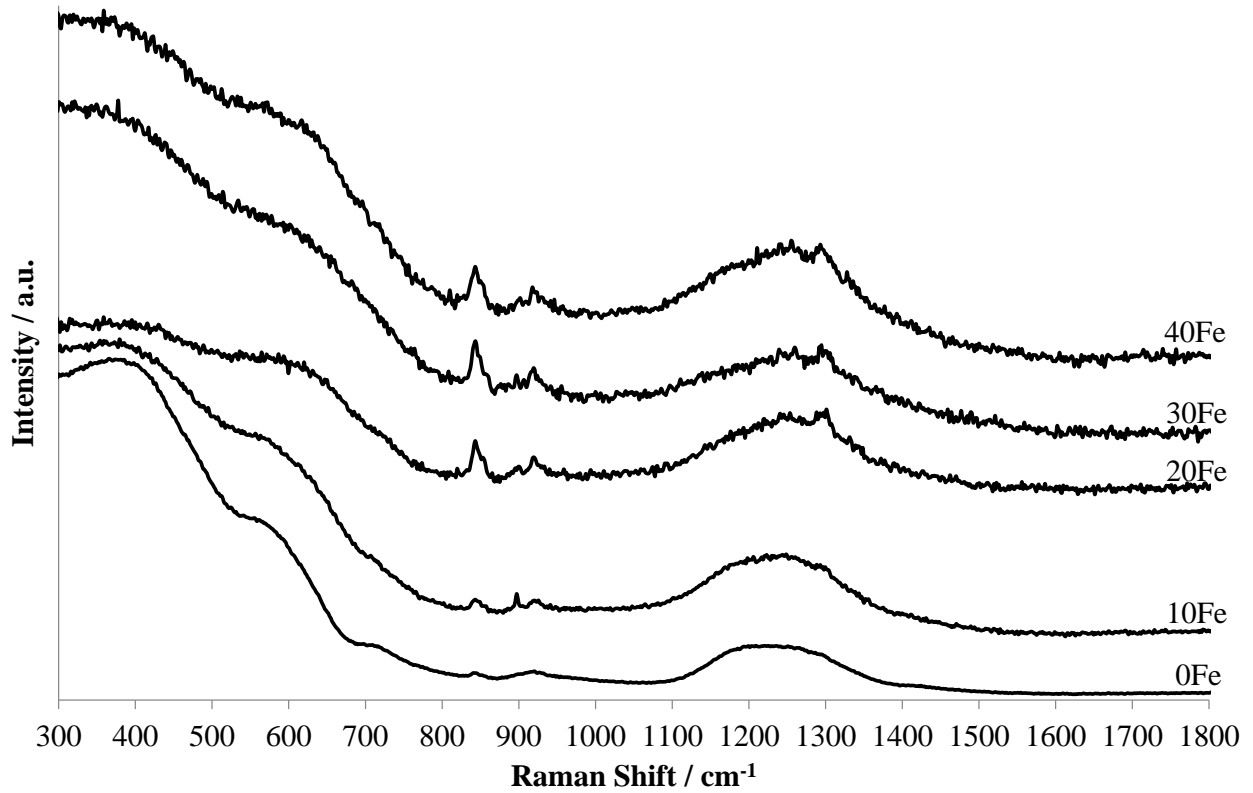
Table 2. IR and Raman band assignments

IR / cm^{-1}	Raman / cm^{-1}	Structural origin	References
-	400	Bi-O-Bi + Bi-O in [BiO$_6$] units.	[17, 18, 23, 32, 33]
-	620	Bi-O$^-$ (NBO) stretching vibration	[17, 18, 33]
720	720	B-O-B bending in trigonal BO$_3$ units	[18, 32, 33, 34]
-	840	Bi-O in pyramidal (BiO$_3$) units and B-O in (BO$_4$) units	[18, 32, 33]
880		Bi-O / Bi-O-Bi in BiO$_6$ octahedra	[18]
	920	B-O in trigonal (BO$_3$) units	[18]
900-950	-	Stretching vibration of (BO$_4$) units	[32, 33, 35]
1150-1170	1180	B-O in tetrahedral (BO$_4$) units	[18, 34]
1200-1300	1280	B-O of (BO$_3$) triangles	[18, 23, 32, 34, 36]

Table 3. Fitted Mössbauer parameters for samples 20Fe to 40Fe

Sample	Fitting Reduced χ^2	Centre Shift $\pm$ 0.02 / mm s^{-1}	Quadrupole Splitting $\pm$ 0.02 / mm s^{-1}	Linewidth HWHM $\pm$ 0.02 / mm s^{-1}
20Fe	0.517	0.31	0.88	0.26
30Fe	0.621	0.34	0.86	0.27
40Fe	0.493	0.32	0.90	0.23

Figure 6. Fitted Mössbauer spectra for samples 20Fe to 40Fe

Figure 6. Fitted Mössbauer spectra for samples 20Fe to 40Fe
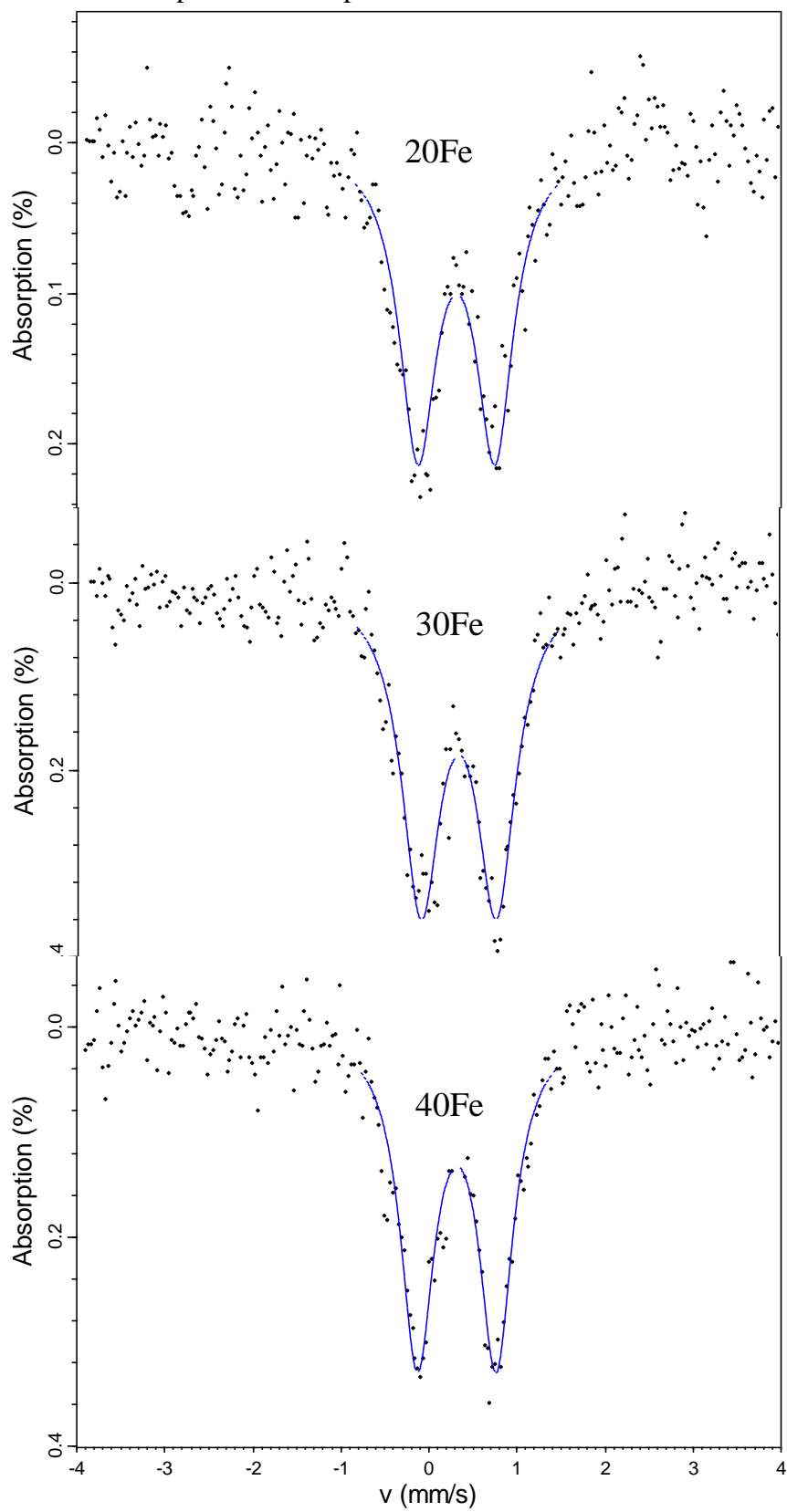
4. Discussion

Other researchers [25-27] have studied the same nominal base glass composition as ours (80 mol% Bi_2O_3 – 20 mol% B_2O_3). Yawale and Pakade [25] melted their glasses at 1273 - 1773 K for 2 hours in fireclay (aluminosilicate) crucibles and obtained a density of 7.701 g cm^{-3}. On the other hand, Stehle *et al.* [26] melted their glass at considerably lower temperatures and times (1273 K for 10 minutes) in platinum crucibles and obtained a density of ~8.5 ± 0.2 g cm^{-3}. Our measured density of 7.88 ± 0.01 g cm^{-3} for glass melted in an Al_2O_3 crucible at 1373 K for 30 min lies between these literature data. The differences in measured densities are likely to be principally due to different levels of contamination from corrosion of the crucible material (negligible for platinum [26, 27]; contamination from Al_2O_3 (this study) and fireclay [25]). There may also be contributions from different levels of volatilisation loss on account of differences in melting time and temperature (lowest for 1273 K / 10 minutes [26]; slightly higher for 1373 K / 30 minutes (this study); higher for 1273 - 1773 K for 10 minutes [27]; and considerably higher for 1273 - 1773 K for 2 hours [25]. Whilst none of these other authors [25-27] chemically analysed their glasses, Stehle *et al.* [26] did carry out "weight loss measurements to ensure stoichiometric accuracy". It is thus reasonable to assume that their glasses exhibit as close to the true density of glasses with the composition 80 mol% Bi_2O_3 – 20 mol% B_2O_3, free from contamination, and produced under the roller quenching preparation conditions they used, as can be achieved experimentally. All of our glasses were found to contain ~1 to 2 wt% (~4 to 7 mol%) Al_2O_3, as detected by standardless XRF analysis and shown in Table 1. The limited accuracy of XRF IQ+ program makes it difficult to gauge boron losses, as may reasonably be expected to occur at some level, through consideration of the contents of the other main components, Bi_2O_3 and Fe_2O_3. However, we note that whilst the analysed Bi_2O_3 contents are lower than their nominal values for samples 0Fe and 10Fe, they are above their nominal values for samples 20Fe and 30Fe. Consequently, and also taking into account the analysed Al_2O_3 contents of the glasses which will reduce the contents of all other components proportionately, we can conclude that boron losses, whilst not necessarily negligible, were not high.

Thermal analysis results clearly show that modest replacement of Bi_2O_3 by Fe_2O_3 (10-20 mol %) results in a significant expansion of the temperature range between T_g and T_x, from 32 K in the iron-free glass which essentially doubles to 66 K in the 10 mol % Fe_2O_3 glass. Further

replacements of Bi_2O_3 by Fe_2O_3 (20-40 mol%) result in decreases in ΔT from this maximum – however, even at 40 mol% Fe_2O_3, the value of ΔT is still larger than for the iron-free 20 B_2O_3 – 80 Bi_2O_3 glass. The increasing suppression of the endothermic event observed upon increasing additions of iron suggest frustration of crystallisation, producing multiple phases, as evidenced by the multiple weak crystallisation / melting peaks at temperatures above ca. 823 K in the DTA traces for the iron-containing samples. The extracted thermal stability and glass formation criteria ΔT, S and K_{gl} are all consistent with the view that partial replacement of Bi_2O_3 by Fe_2O_3, especially at 10 and 20 mol % replacement, enhanced glass formation and thermal stability. Comparison of extracted thermal properties ΔT, S and K_{gl} with data for similar glasses from literature shows that the obtained thermal parameters for the 80 Bi_2O_3 – 20 B_2O_3 base glass (Sample 0Fe) are consistent with the trends observed by Shaaban *et al.* [14] for glasses with compositions xBi_2O_3 – $(100 − x)B_2O_3$ with x = 35 to 60 mol%; and with Cheng *et al.* [32] for glasses with compositions xBi_2O_3 – $(100 − x)B_2O_3$ with x = 30 to 60 mol%. Increasing Bi_2O_3 content in all series lead to decreased ΔT and K_{gl}, and similar values of S, indicating a trend of decreasing glass stability. For example, Shaaban's 60 Bi_2O_3 – 40 B_2O_3 glass gave ΔT = 56K, S = 0.954 and K_{gl} = 0.386; and Cheng's 60 Bi_2O_3 – 40 B_2O_3 glass gave ΔT = 68K and K_{gl} = 0.42 whilst our 80 Bi_2O_3 – 20 B_2O_3 glasses give ΔT = 32K, S = 1.061 and K_{gl} = 0.142, confirming the trend in decreasing glass stability with increasing Bi_2O_3 content and decreasing B_2O_3 content, which is consistent with Stehle *et al.* [26]. However, in our samples, the introduction of Fe_2O_3 leads to a rapid increase in glass stability wherein the composition 70 Bi_2O_3 – 20 B_2O_3 – 10 Fe_2O_3 gave ΔT = 66K, S = 1.455 and K_{gl} = 0.420, which is more stable than Shaaban's 60 Bi_2O_3 – 40 B_2O_3 glass and has the same stability as Cheng's 60 Bi_2O_3 – 40 B_2O_3 glass. Our 60 Bi_2O_3 – 20 B_2O_3 – 20 Fe_2O_3 is also more stable than Shaaban's 60 Bi_2O_3 – 40 B_2O_3 glass, with ΔT = 61K, S = 2.948 and K_{gl} = 0.305. Study of the data of Stehle *et al.* [26] for binary Bi_2O_3-B_2O_3 glasses enables further comparison of the effect of Fe_2O_3 addition vs. B_2O_3 addition. Stehle *et al.* [26] illustrated the difference between "the crystallisation temperature T_x" and onset T_g. In the absence of any description by Stehle *et al.* [26] as to whether their "T_x" refers to onset crystallisation temperature (T_x in this study) or crystallisation peak temperature (T_c in this study), we have assumed, by comparison with our data, that their "crystallisation temperature T_x" is the crystallisation peak temperature (T_c in this study). Based on this assumption, Stehle's T_c-T_g increased from ~58 K for 80 Bi_2O_3 – 20 B_2O_3 glass to ~70 K for 70 Bi_2O_3 – 30 B_2O_3 glass, to

~115 K for 60 Bi_2O_3 – 40 B_2O_3 glass. By comparison our glasses with nominal 80, 70 and 60 mol% Bi_2O_3 contents exhibited T_c - T_x of 52, 80 and 93 K, which also mirror this trend of increasing (T_x-T_g) with decreasing Bi_2O_3 content, and are of similar magnitude. This in turn indicates that the improvements in (T_x-T_g) obtained by partially replacing Bi_2O_3 by B_2O_3 are mirrored by the improvements in (T_x-T_g) resulting from partially replacing Bi_2O_3 by (Fe_2O_3 + Al_2O_3). The effects of Al_2O_3, in addition to Fe_2O_3, must be considered for our glasses, since XRF analysis confirmed the presence of ~ 4 to 7 ($\pm$ 3) mol % Al_2O_3. Previously it was shown that similar additions (5 mol%) of Al_2O_3 can improve the thermal stability of iron phosphate glasses [37]. In addition to this, increasing the number of different elements in a glass is well known to frustrate crystallisation. It is therefore likely that the levels of Al_2O_3 present in our glasses have an impact on thermal stability. A substantial number of researchers describing similar glasses also prepared their glasses in refractory crucibles (or did not state the crucible material) – and therefore it is suggested that other such glasses may have also contained similar, or greater, impurity levels of Al_2O_3 [14, 16, 17, 18, 21, 23]. Since Al_2O_3 contents of all glasses studied here remain at broadly similar levels, including the 80 Bi_2O_3-20 B_2O_3 base glass, it can be concluded that the improvements in thermal stability, compared with the base glass, that are observed in this study are as a result of partially replacing Bi_2O_3 by Fe_2O_3 and not Al_2O_3 contamination. The increases in T_d with increasing Fe_2O_3 content are consistent with partial replacement of Bi^{3+} by Fe^{3+}, as the corresponding dissociation energies of Fe_2O_3 (287 kcal / mol) and Bi_2O_3 (147 kcal / mol) [38] are consistent with a more rigid glass network requiring higher temperatures to initiate viscous flow, as Fe_2O_3 increasingly replaces Bi_2O_3.

The eutectic temperature in the Bi_2O_3-$2Bi_2O_3.B_2O_3$ subsystem, in which the 80 mol% Bi_2O_3 – 20 mol% B_2O_3 (sample 0Fe) composition is located, has a T_m of 622°C (895 K) [39, 40]. According to a more recent version of the Bi_2O_3-B_2O_3 phase diagram [41] the 80 mol% Bi_2O_3 – 20 mol% B_2O_3 composition is very close to the eutectic composition of the Bi_2O_3-$5:3Bi_2O_3:B_2O_3$ subsystem. Our T_m of 588°C found in this work for sample 0Fe has an intermediate value, although the glass is actually ternary, since it contains Al_2O_3, which may explain the observed, modest difference in T_m from the previous work. The other compositions studied here are quaternary as both Fe_2O_3 and Al_2O_3 must be considered.

When considering the structure of the B_2O_3-Bi_2O_3-Fe_2O_3-Al_2O_3 glasses studied here, it is important to first consider the structure of binary B_2O_3-Bi_2O_3 glasses. Maeder [1] summarised a

number of studies of high-bismuth borate glasses, and in particular, Bajaj *et al.* [13] and Dimitrov and Komatsu [42], using ^{11}B MAS-NMR, provided evidence strongly suggesting that over 80 % of the boron in very-high lead and bismuth borate glasses (i.e. in all glasses studied here) will adopt trigonal coordination; and consequently the amount of four-coordinated B^{3+} is expected to be small. Bismuth in $Bi_2O_3 - B_2O_3$ glasses has been described as occupying (BiO_6) octahedral sites [1, 17, 18, 23, 32, 33]. All Raman spectra (Figure 5) show bands due to bridged anion modes at ca. 400 cm^{-1}. The Raman band at ca. 600 cm^{-1} is attributed to Bi-O[-] stretching (vibration of bismuth - non-bridging oxygen) in (BiO_6) polyhedra [17, 18, 33]. The IR band at 720 cm^{-1} is attributed to bending vibrations of B–O–B trigonal units [18, 32, 33, 34]. The weak IR band at 920 cm^{-1} has been attributed to stretching vibrations of (BO_4) units [32, 33, 35]. The IR and Raman bands centred at 1180 cm^{-1} and 1280 cm^{-1} are a matter of debate, as they have received little prior attention as discrete units in the context of very high -PbO or -Bi_2O_3 borate glasses. However, it is clear that Raman bands at high frequency (ca. 1250 cm^{-1}) provide information on short range order in these borate glass systems.

Aside from the overall intensity of Raman-active bands being suppressed by Fe_2O_3 additions, the spectral changes that do occur upon increasing Fe_2O_3 addition, in both FT-IR and Raman spectra, are surprisingly subtle, with no large changes. Overlaying the FT-IR spectra on each other reveals little difference between any of the sample spectra. Overlaying the Raman spectra, when amplified sufficiently to counteract the suppressing effect of Fe_2O_3 additions (as in Figure 5), shows only the band at 720 cm^{-1} being incorporated into the stronger background occurring at low Raman shifts, and a small change in the relative intensities of the two overlapping Raman bands at 1180 cm^{-1} and 1280 cm^{-1}, which manifests as a change in the overall peak profile in this spectral region.

The splitting of both the high-frequency IR band and the high-Raman shift band into bands at 1180 and 1280 cm^{-1} can be observed in the data of several authors [14, 17, 18, 33, 34, 35, 36, 43, 44]. However, few have specifically discussed this band splitting. It was discussed by Kotkova *et al.* [43], who also observed band splitting for PbO-Bi_2O_3-B_2O_3 glasses with high (Pb+Bi) contents. They noted that the band at 1180 cm^{-1} is often stated to indicate of the presence diborate groups, but that it is unlikely that diborate groups form at such high modifier contents. They attributed both Raman bands, at 1180 cm^{-1} and 1280 cm^{-1} to trigonal borate groups. However, others have attributed the band at 1180 cm^{-1} to tetrahedral borate groups [18,

34]. Assuming this is the correct assignment in the case of our glasses, then our results suggest a modest increase in the $^{[3]}B^{3+}$ / $^{[4]}B^{3+}$ ratio with increasing Fe_2O_3 content. However, as previously noted, evidence from other studies indicates that the large majority (> 80%) of the boron in our glasses is likely to be trigonally-coordinated $^{[3]}B^{3+}$, so further research would be required to confirm the abundance of tetrahedral $^{[4]}B^{3+}$ and its compositional dependence, and to relate this back to the IR and Raman spectra. On balance, the majority of literature suggests that both the 1180 cm^{-1} and 1280 cm^{-1} IR and Raman bands are related to trigonal $^{[3]}B^{3+}$.

The suppressing effect of Fe_2O_3 concentration on Raman spectra that we have observed here are also mirrored in other, related studies. Kotkova *et al.* [43] showed similar suppression with increasing PbO concentration in $(PbO)_x(Bi_2O_3)_{0.2}(B_2O_3)_{0.8-x}$ glasses and Ardelean and Cora [33] showed comparable behaviour with increasing CuO concentration in $xCuO.(100-x)(3Bi_2O_3-B_2O_3)$ glasses. Research by Pan *et al.* [45], who studied a wide range of B_2O_3-PbO glasses, showed that the Raman scattering cross-section increased strongly with increasing PbO content, with this increase dominating in the low-frequency region. This behaviour was attributed in part to the polarizability of Pb^{2+} cations. Since Bi^{3+} is also highly polarisable, one possible cause of the suppression of Raman spectra upon increasing Fe_2O_3 content in our glasses is that the Fe_2O_3 partially replaced Bi_2O_3 and consequently the Raman cross-section of the glass became considerably weaker.

The Centre Shift (CS) and Quadrupole Splitting (QS) values obtained from fitting of Mössbauer spectra are consistent with the Fe^{3+} oxidation state in oxide glasses [47-53] and there is no evidence for any measurable levels of Fe^{2+} in any of the glasses studied here. The coordination of the Fe^{3+} ions identified can be determined qualitatively from CS and QS values. With CS of 0.31-0.34 mm s^{-1} and QS of 0.86-0.90 mm s^{-1} these values lie on the tetrahedral side of, but very close to, the boundary between 4-coordination and higher coordination numbers of 5 and 6 [47-50]. The associated Linewidth (LW) values of 0.23-0.27 mm s^{-1} are consistent with a range of site distortions, as occur in oxide glasses. It is therefore highly likely that whilst some Fe^{3+} adopts tetrahedral coordination with respect to oxygen, a substantial fraction of Fe^{3+} occupies 5- and / or 6- coordinated sites in these glasses: this is consistent with literature for a wide range of borate glasses [47-53]. The fact that the obtained Mössbauer CS, QS and LW parameters do not change significantly between 20%, 30% and 40% Fe_2O_3 nominal content of the glasses studied, suggests that the Fe^{3+} local environments, range of site occupations and

range of site distortions, are little affected by the compositional variations studied. This is less common, but not unique, for borate glasses: previous studies of related glasses [46, 51-53] have indicated changes in Mössbauer parameters with different Fe_2O_3 contents. However, equivalent findings to ours were also reported by Akamatsu *et al*. [22] for $xFe_2O.(80 - x)Bi_2O_3.20.B_2O_3$ glasses where (18.2 ≤ x ≤ 40.0), which are closely similar in composition to our glasses. Akamatsu *et al.* [22] also reported Centre Shift values of 0.32 mm s^{-1}, and only Fe^{3+} was present in their glasses, again in close agreement with our results. Other compositionally-relevant Mössbauer results from literature also include lead borate glasses [51-53] which included high-PbO, low-B_2O_3 glasses containing varying amounts of Fe_2O_3. Sekhon and Kamal [52, 53] observed an approximately monotonic decrease in Fe^{3+} Centre Shift with increasing PbO contents of up to 85mol% PbO in x PbO.(1-x) B_2O_3 glasses containing 10 mol% Fe_2O_3. They attributed this to formation of Fe—O—Pb bonds replacing Fe—O—B bonds with increasing PbO content. Burzo and Ardelean [51] also observed a decrease in Fe^{3+} Centre Shift, here with increasing Fe_2O_3 content from 5 to 50 mol% in $xFe_2O_3.1-x(PbO.3B_2O_3)$ glasses. These works do not readily enable direct and unambiguous comparisons with our data, since Sekhon and Kamal [52, 53] considered a fixed Fe_2O_3 content and boron-rich glasses; and Burzo and Ardelean [45] studied boron-rich glasses. Moreover, the iron in some of their glasses occurred in both Fe^{2+} and Fe^{3+} oxidation states, whereas all of the iron in our glasses occurred as Fe^{3+}. Nevertheless, the lack of change in Mössbauer parameters with increasing Fe_2O_3 content of our glasses does enable useful inferences on glass structure. As discussed previously, it is suggested that the large majority (over 80%) of the boron in our glasses occupies trigonal coordination. Consequently the trigonal boron does not require nearby modifier cations for charge balance or stabilisation, and therefore it is less likely that Fe – O – B bonds would be required. However, the tetrahedral fraction of the Fe^{3+} would require nearby cations for charge balance and stabilisation and, moreover, it may be expected that the majority of the Al^{3+} present in these glasses would also require charge balance and stabilisation. This suggests that Fe^{3+} would be more likely to form Fe – O – Bi bonds for any charge balance / stabilisation that may be required, and since there is an abundance of Bi^{3+} in all glasses studied, this may explain the high stability and invariance with composition of the Fe^{3+} sites in these glasses. It is also highly likely that $Fe^{3+} – O – Fe^{3+}$ bonds (clustering) will also be present in these glasses due to their high iron contents. Such behaviour has previously been observed for other borate glasses with lower Fe_2O_3 contents than studied

here [54, 55] and recently, Akamatsu *et al.* [22], who studied glasses with closely similar compositions to ours, showed that magnetic clusters become more significant as Fe_2O_3 content increases. They also used transmission electron microscopy to show that the magnetic clusters were not nanocrystals but were an Fe-rich amorphous phase. This suggests that sub-nanophase separation occurred in their glasses and, owing to the close compositional similarities between our glasses and those of Akamatsu *et al*. [22], we can surmise that it may have also occurred in the Fe-doped glasses studied here.

5. Conclusions

Glasses with nominal molar composition $20B_2O_3 - (80-x)Bi_2O_3 - xFe_2O_3$ (where x = 0–40) were successfully prepared by melt-quenching. Spectroscopic studies have confirmed the presence of BO_3 and BiO_6 structural units in all glasses, with glass structure apparently little affected by iron, which is solely present in the Fe^{3+} oxidation state in all glasses, adopting a distribution of coordinations from 4 to 6. Thermal stability, measured by a number of different parameters, was greatly improved by iron additions, with maximum improvements achieved with 10-20 mol% Fe_2O_3 addition. These improvements are accompanied by modest increases in T_g and T_d. Consequently it is shown that partial replacement of Bi_2O_3 by 10 -20 mol% Fe_2O_3 provides a large improvement in thermal stability of B_2O_3-Bi_2O_3 glasses, benefitting the design of new bismuth borate based glasses for low-temperature applications such as sealing.

6. Acknowledgements

22

References

[1] T. Maeder, Review of Bi_2O_3 based glasses for electronics and related applications, *International Materials Reviews* 58 (2013) 3-40.

[2] R. G. Frieser, A review of solder glasses, *Electrocomponent Science and Technology* 2 (1975) 163-199.

[3] T. Takamori, Solder Glasses, Chapter 5 in: Glass II - Treatise on Materials Science and Engineering, Volume 17, Edited by M. Tomozawa and R. H. Doremus, Academic Press, New York, 1979, pp. 173 – 255.

[4] I. W. Donald, Glass-to-metal seals, Society of Glass Technology, Sheffield, 2009.

[5] D. R. Uhlmann and R. R. Shaw, The thermal expansion of alkali borate glasses and the boric oxide anomaly, *Journal of Non-Crystalline Solids* 1 (1969) 347-359.

[6] J. E. Shelby, Thermal expansion of alkali borate glasses, *Journal of the American Ceramic Society* 66 (1983) 225-227.

[7] S. Suzuki and Y. Abe, The free volume of some oxide glasses at their transition temperature, *Journal of Non-Crystalline Solids* 43 (1981) 141-143.

[8] A. Ahmed and A. Abbas, Mixed-alkali effect in alkali borate glasses, *Journal of Non-Crystalline Solids* 80 (1986) 371-378.

[9] I. Wozniak and P. F. James, Glasses with low softening points in the Na_2O-BaO-B_2O_3, NaF-BaO-B_2O_3 and BaO-B_2O_3-V_2O_5 systems, *Glass Technology* 25 (1984) 98-104.

[10] A. Ide, Low melting glass, sealing composition and sealing paste, U. S. Patent No. 7,291,573, 6 November 2007.

[11] D. Goedeke and P. Brix, Low-melting lead-free solder glass and uses thereof, U. S. Patent No. 7,799,712 B2, 21 September 2010.

[12] H. Usui, T. Manabe, K. Harada and R. Tanabe, Hermetic sealing composition, U. S. Patent No. 5,733,828, 31 March 1998.

[13] A. Bajaj, A. Khanna, B. Chen, J. G. Longstaffe, U-Werner Zwanziger, J. W. Zwanziger, Y. Gómez and F. González, Structural investigation of bismuth borate glasses and crystalline phases, *Journal of Non-Crystalline Solids* 355 (2009) 45-53.

[14] E. R. Shaaban, M. Shapaan and Y. B. Saddeek, Structural and thermal stability criteria of Bi_2O_3-B_2O_3 glasses, *Journal of Physics: Condensed Matter* 20 (2008) 155108.

[15] W. H. Dumbaugh, Heavy metal oxide glasses containing Bi_2O_3, *Physics and Chemistry of Glasses* 27 (1986) 119-123.

[16] H.H. Qiu, T. Ito, H. Sakata, DC conductivity of Fe_2O_3-Bi_2O_3-B_2O_3 glasses, *Materials Chemistry and Physics* 58 (1999) 243-248.

[17] L. Baia, R. Stefan, J. Popp, S. Simon and W. Kiefer, Vibrational spectroscopy of highly iron doped B_2O_3–Bi_2O_3 glass systems, *Journal of Non-Crystalline Solids* 324 (2003) 109-117.

[18] L. Baia, R. Stefan, W. Kiefer and S. Simon, Structural characteristics of B_2O_3–Bi_2O_3 glasses with high transition metal oxide content, *Journal of Raman Spectroscopy* 36 (2005) 262-266.

[19] A. Al Hajry, A. A. Soliman and M. M. El-Desoky, Electrical and thermal properties of semiconducting Fe_2O_3–Bi_2O_3–$Na_2B_4O_7$ glasses, *Thermochimica Acta* 427 (2005) 181–186.

[20] M. M. El-Desoky, N. M. Tashtoush and H. Habib, Characterization and electrical properties of semiconducting Fe_2O_3–Bi_2O_3–$K_2B_4O_7$ glasses, *Journal of Materials Science* 16 (2005) 533–539.

[21] M. M. El-Desoky and A. Al Shahrani, Iron doping of semiconducting bismuth alkali borate glasses, *Physica B* 383B (2006) 163–170.

[22] H. Akamatsu, K. Tanaka, K. Fujita and S. Murai, Magnetic phase transitions in Fe_2O_3–Bi_2O_3–B_2O_3 glasses, *Journal of Physics: Condensed Matter* 20 (2008) 235216.

[23] F. H. El-Batal, M. A. Marzouk and A. M. Abdel Ghany, Gamma rays interaction with bismuth borate glasses doped by transition metal ions, *Journal of Materials Science* 46 (2011) 5140-5152.

[24] M.A. Marzouk, F.H. El-Batal, W.H. Eisa and N.A. Ghoneim, Comparative spectral and shielding studies of binary borate glasses with the heavy metal oxides SrO, CdO, BaO, PbO or Bi_2O_3 before and after gamma irradiation, *Journal of Non-Crystalline Solids* 387 (2014) 155-160.

[25] S. P. Yawale and S. V. Pakade, D. C. conductivity and hopping mechanism in Bi_2O_3-B_2O_3 glasses, *Journal of Materials Science* 28 (1993) 5451-5455.

[26] C. Stehle, C. Vira, D. Hogan, S. Feller and M. Affatigato, Optical and physical properties of bismuth borate glasses related to structure, *Physics and Chemistry of Glasses* 39 (1998) 83-86.

[27] H. B. George, C. Vira, C. Stehle, J. Meyer, S. Evers, D. Hogan, S. Feller and M. Affatigato, A structural analysis of the physical properties of bismuth and lead based glasses, *Physics and Chemistry of Glasses* 40 (1999) 326-332.

[28] A. Dietzel, Glass structure and glass properties, *Glastechnische Berichte* 22 (1968) 41–48.

[29] M. Saad and M. Poulain, Glass forming ability criteria, *Materials Science Forum* 19-20 (1987) 11-18.

[30] A. Hruby, Evaluation of glass-forming tendency by means of DTA, *Czechoslovak Journal of Physics B* 22 (1972) 1187-1193.

[31] D. Rancourt, Recoil Mössbauer Spectral Analysis Software, Intelligent Scientific Applications Inc., Ottawa, (1998).

[32] Y. Cheng, H. Xiao, W. Guo and W. Guo, Structure and crystallization kinetics of Bi_2O_3–B_2O_3 glasses, *Thermochimica Acta* 444 (2006) 173–178.

[33] I. Ardelean and S. Cora, FT-IR, Raman and UV-Vis spectroscopic studies of copper doped $3Bi_2O_3.B_2O_3$ glass matrix, *Journal of Materials Science: Materials Electronics* 19 (2008) 584-588.

[34] S. R. Rejisha and N. Santha, Structural investigations on $20MO-xBi_2O_3-(80-x)B_2O_3$ (M=Ca, Sr and Ba; x=15 and 55) glasses, *Journal of Non-Crystalline Solids* 357 (2011) 3813-3821.

[35] C. Gautam, A. K. Yadav and A. K. Singh, A review of infrared spectroscopy of borate glasses with effects of different additives, *International Scholarly Research Network Ceramics* (2012) 428497.

[36] W. A. Pisarski, J. Pisarska, G. Dominiak-Dzik, M. Maczka and W. Ryba-Romanowski, *Journal of the Physics and Chemistry of Solids* 67 (2006) 2452-2457.

[37] P. A. Bingham, R. J. Hand and S. D. Forder, Doping of iron phosphate glasses with Al_2O_3, SiO_2 or B_2O_3 for improved thermal stability, *Materials Research Bulletin* 41 (2006) 1622-1630.

[38] K. H. Sun and M. L. Huggins, Energy additivity in oxygen-containing crystals and glasses II, *Journal of Physical Chemistry* 51 (1947) 438–443.

[39] E. M. Levin and C. L. McDaniel, The system Bi_2O_3 - B_2O_3, *Journal of the American Ceramic Society* 45 (1962) 355-360.

[40] M. Burianek and M. Mühlberg, Crystal growth of boron sillenite $Bi_{24}B_2O_{39}$, *Crystal Research Technology* 32 (1997) 1023-1027.

[41] Yu F. Kargin, V. P. Zhereb and A. V. Egorysheva, Metastable phase diagram for the Bi_2O_3 - B_2O_3 system, *Russian Journal of Inorganic Chemistry* 47 (2002) 1240-1242.

[42] V. Dimitrov and T. Komatsu, Average single bond strength and optical basicity of Bi_2O_3–B_2O_3 and Sb_2O_3–B_2O_3 glasses, *Journal of Non-Crystalline Solids* 356 (2010) 258–262.

[43] K. Kotkova, H. Ticha and L. Tichy, Raman studies and optical properties of some $(PbO)_x(Bi_2O_3)_{0.2}(B_2O_3)_{0.8-x}$ glasses, *Journal of Raman Spectroscopy* 39 (2008) 1219-1226.

[44] B. N. Meera, A. K. Sood, N. Chandrabhas and J. Ramakrishna, Raman study of lead borate glasses, *Journal of Non-Crystalline Solids* 126 (1990) 224-230.

[45] Z. Pan, S. H. Morgan and B. H. Long, Raman scattering cross-section and non-linear optical response of lead borate glasses, *Journal of Non-Crystalline Solids* 185 (1995) 127-134.

[46] M. D. Dyar, A review of Mössbauer data on inorganic glasses: the effects of composition on iron valency and coordination, *American Mineralogist* 70 (1985) 304-316.

[47] T. Nishida, Advances in the Mössbauer effect for the structural study of glasses, *Journal of Non-Crystalline Solids* 177 (1994) 257-268.

[48] G. Tomandl, Mössbauer effect in glasses, Ch. 5 in Glass: Science and Technology, vol. 4B, Ed. D. R. Uhlmann and N. J. Kriedl, Academic Press, New York (1990).

[49] S. S. Sekhon and R. Kamal, Applications of Mössbauer spectroscopy to the study of inorganic oxide glasses, *Physics and Chemistry of Glasses* 29 (1988) 157-167.

[50] M. D. Dyar, D. G. Agresti, M. W. Schaefer, C. A. Grant and E. C. Sklute, Mössbauer spectroscopy of Earth and planetary materials, *Annual Reviews in Earth and Planetary Sciences* 34 (2006) 83–125.

[51] E. Burzo and I. Ardelean, Mössbauer effect study of iron cations in lead borate glasses, *Physics and Chemistry of Glasses* 20 (1979) 15-20.

[52] S. S. Sekhon and R. Kamal, Mössbauer study in the glass system $PbO.2B_2O_3.Fe_2O_3$, *Journal of Non-Crystalline Solids* 32 (1978) 189-192.

[53] S. S. Sekhon and R. Kamal, Mössbauer spectra in x $PbO.(1-x)$ B_2O_3 doped with Fe_2O_3, *Journal of Non-Crystalline Solids* 33 (1979) 169-175.

[54] K. Tanaka, K. Kamiya, T. Yoko, S. Tanabe, K. Hirao and N. Soga, Electron spin resonance study of iron ion clusters in borate glasses, *Physics and Chemistry of Glasses* 32 (1991) 16-21.

[55] M. A. Valente and S. K. Mendiratta, Magnetic susceptibility and aspects of magnetic interaction in Gd, Fe, and mixed Gd-Fe lead borate glasses, *Physics and Chemistry of Glasses* 33 (1992) 149-153.